國內圖書館　期刊複印< 申請件明細 >

申請件編號(NDDS NO.):	10362602
申請日期(Request Date):	11/28/2022 10:05
申請人姓名(Patron Name):	大里仁愛醫院
申請館(Borrower):	仁愛醫療財團法人圖書室
期刊類別(Journal Type):	西文期刊(Western Journals)
期刊名(Journal Title):	Journal of NeuroInterventional Surgery
篇　名(Article Title):	Prediction of cerebral aneurysm rupture using a point cloud neural network.
作　者(Article Author):	Luo X, Wang J, …
卷號(Volume):	14
期號(Number):	4
起頁(Start page):	-
訖頁(End page) :	-
出版年(Year):	2022
ISBN/ISSN:	1759-8478
DOI/PMID:	
國內無則轉國外:	否
可接受的金額:	
被申請館(一)(Lender1):	長庚紀念醫院林口圖書館
退件理由一(Rejection1):	
被申請館(二)(Lender2):	
退件理由二(Rejection2):	
被申請館(三)(Lender3):	
退件理由三(Rejection3):	
傳遞方式(Delivery Method):	NDDS Express
申請時限(Needed By):	前提供,否則請取消本案
收據(Receipt):	是(Yes)
收據抬頭(Receipt Title):	仁愛醫療財團法人
備註(Notes):	J Neurointerv Surg. 2022 Apr 8;neurintsurg-2022-018655. doi: 10.1136/neurintsurg-2022-018655. Online ahead of print. 無頁數顯示
資料提供方式(SentVia):	NDDS Express
申請狀態(Status):	申請館待收
影印頁數(Pages):	8
影印費用(Photocopy):	0
手續費(Handling):	0
傳真費用(Fax):	0
郵資費用(Postage):	0
其他費用(Others):	0
總共費用(Total):	0
被申請館註記:	

Original research

Prediction of cerebral aneurysm rupture using a point cloud neural network

Xiaoyuan Luo,[1] Jienan Wang,[2] Xinmei Liang,[3] Lei Yan,[4] XinHua Chen,[5] Jian He,[6] Jing Luo,[7] Bing Zhao ,[8] Guangchen He,[2] Manning Wang,[1] Yueqi Zhu [2]

► Additional supplemental material is published online only. To view, please visit the journal online (http://dx.doi.org/10.1136/neurintsurg-2022-018655).

For numbered affiliations see end of article.

Correspondence to
Dr Yueqi Zhu, Department of Radiology, Shanghai Jiaotong University Affiliated sixth People's Hospital, Shanghai, China; zhuyueqi@hotmail.com
Dr Manning Wang; mnwang@fudan.edu.cn

XL and JW contributed equally.

Received 6 January 2022
Accepted 27 March 2022

ABSTRACT

Objective Accurate prediction of cerebral aneurysm (CA) rupture is of great significance. We intended to evaluate the accuracy of the point cloud neural network (PC-NN) in predicting CA rupture using MR angiography (MRA) and CT angiography (CTA) data.

Methods 418 CAs in 411 consecutive patients confirmed by CTA (n=180) or MRA (n=238) in a single hospital were retrospectively analyzed. A PC-NN aneurysm model with/without parent artery involvement was used for CA rupture prediction and compared with ridge regression, support vector machine (SVM) and neural network (NN) models based on radiomics features. Furthermore, the performance of the trained PC-NN and radiomics-based models was prospectively evaluated in 258 CAs of 254 patients from five external centers.

Results In the internal test data, the area under the curve (AUC) of the PC-NN model trained with parent artery (AUC=0.913) was significantly higher than that of the PC-NN model trained without parent artery (AUC=0.851; p=0.041) and of the ridge regression (AUC=0.803; p=0.019), SVM (AUC=0.788; p=0.013) and NN (AUC=0.805; p=0.023) radiomics-based models. Additionally, the PC-NN model trained with MRA source data achieved a higher prediction accuracy (AUC=0.936) than that trained with CTA source data (AUC=0.824; p=0.043). In external data of prospective cohort patients, the AUC of PC-NN was 0.835, significantly higher than ridge regression (0.692; p<0.001), SVM (0.701; p<0.001) and NN (0.681; p<0.001) models.

Conclusion PC-NNs can achieve more accurate CA rupture prediction than traditional radiomics-based models. Furthermore, the performance of the PC-NN model trained with MRA data was superior to that trained with CTA data.

Key messages

What is already known on this topic

► The number of incidentally discovered unruptured cerebral aneurysms in the clinic setting has increased, but their rupture risk remains unclear. Our study intends to use a new artificial intelligence model point cloud neural network (PC-NN) to investigate the accuracy of aneurysm rupture prediction.

What this study adds

► The PC-NN model trained with parent artery involvement and MR angiography source data was of great help to improve its prediction accuracy.
► The PC-NN model was proved to be superior to other radiomics models in predicting aneurysm rupture in both internal and external test data.

How this study might affect research, practice or policy

► The PC-NN model may become a supportive and complementary tool to provide individualized treatment plans for patients with cerebral aneurysm in the clinic setting.

INTRODUCTION

Cerebral aneurysms (CAs) are a common cerebrovascular disease with a prevalence of 1–7% in adults with an annual rupture rate of approximately 1%.[1] In recent years, with the development of non-invasive angiography technologies such as CT angiography (CTA) and MR angiography (MRA), the number of incidentally discovered unruptured CAs has increased. It is of great importance for physicians to identify the stability of CAs in a timely manner before deciding whether to treat them, and to determine the optimal intervention time after balancing the risk of rupture and therapy. The assessment of the stability of a CA involves many factors, including inflammatory,[2] hemodynamic and morphological factors.[3 4] Among them, morphological factors are easily measured, calculated and analyzed and are considered to be directly related to CA rupture; thus, combining morphological factors with clinical features can be used to form a basis by which to judge the stability of a CA.[5]

Many of the morphological features of aneurysms, including the aspect ratio,[6] size ratio, height and bottleneck factor, are considered to be correlated with and have been used to predict aneurysm rupture.[7] In previous studies, rupture prediction models for anterior communicating aneurysms and middle cerebral artery (MCA) aneurysms based on identified independent morphological features demonstrated areas under the curve (AUCs) between 0.80 and 0.829.[5 8] Furthermore, radiomics features automatically extracted by PyRadiomics (version 3.0.1) were used in recent studies to predict CA rupture.[9] Ludwig *et al* applied multivariate analysis based on PyRadiomics-derived features to predict rupture status with an AUC of 0.75.[10] Liu *et al* established different machine learning models based on PyRadiomics-derived features to predict aneurysm stability, the best of which achieved an AUC

To cite: Luo X, Wang J, Liang X, *et al*. *J NeuroIntervent Surg* Epub ahead of print: [*please include* Day Month Year]. doi:10.1136/neurintsurg-2022-018655

of 0.853.[11] These radiomics methods and manually designed features are mainly low-level geometry features based on length or angle.[12] Limited higher-level morphological features have been reported but their effectiveness in rupture status prediction are not well investigated[13 14]; thus, abundant information on the morphological features of CAs and their adjacent parent arteries is not fully utilized. This means that it is difficult to use higher-level information effectively in the context of rupture status prediction.

Recently, point cloud neural networks (PC-NNs) have been proposed in the field of computer vision for learning about rich, high-level geometry features and have been shown to automatically learn thousands of morphological features from massive data compared with existing radiomics-based methods.[15] Therefore, transforming CA image data to point clouds and building a PC-NN model to learn the morphological features from both aneurysms and their parent arteries may improve the accuracy of rupture status prediction. In this study, we generated a point cloud data set on CAs from MRA and CTA data and established a PC-NN model to predict CA rupture based on the learned 1024-dimensional morphological and clinical features. Furthermore, we also compared our PC-NN model with existing radiomics-based methods using test data from a retrospective single center and from five external centers.

METHODS

Patients

This study was approved by the ethics committees of each hospital participating in this study. This study retrospectively included 541 consecutive patients from an internal center and prospectively included 349 patients from five different external centers who were diagnosed with intracranial aneurysms between January 2017 and October 2021. The inclusion criteria were as follows: (1) ruptured or unruptured saccular CAs located in the anterior circulation arteries and, the subarachnoid hemorrhage can be explicitly attributed to aneurysm rupture; (2) a minimum aneurysm diameter >3 mm; and (3) good-quality cerebrovascular imaging—CTA or MRA data—that can adequately be used to reconstruct the aneurysm and 3–5 mm of its adjacent parent arteries with clear boundaries. The exclusion criteria were as follows: (1) non-saccular aneurysms, such as fusiform aneurysms, dissecting aneurysms or pseudoaneurysms; (2) multiple aneurysms that were indistinguishable as the source of hemorrhage; and (3) insufficient image quality to permit accurate image reconstruction or segmentation.

In terms of locations, the CAs were divided into: (1) internal carotid artery (ICA) aneurysms, specifically those located at the clinoidal (C5), ophthalmic (C6) and communicating (C7) segments of the ICA, and posterior communicating artery (PComA) aneurysms; (2) middle cerebral artery (MCA) aneurysms; and (3) anterior cerebral artery (ACA) aneurysms and anterior communicating artery (AComA) aneurysms.

MRA and CTA scan protocol of training data and data preparation

A 3.0 T system (Achieva X Series; Philips Medical Systems, Best, the Netherlands) with a Sense-Head-8 receiver head coil was used. Three-dimensional (3D) time-of-flight (TOF) MR angiograms were obtained by using 3D T1-weighted fast field-echo sequences (repetition time msec/echo time, 35/7 msec; flip angle, 20°; field of view, 250×190×108; four slabs (180 sections); section thickness, 0.8 mm; and matrix, 732×1024). The total acquisition time was 8 min 56 s.[16]

CT angiography was performed with a 64-section spiral CT scanner (Brilliance 64; Philips Healthcare) with the following parameters: tube voltage 120 kV; tube current 333 mA; and rotation speed 0.75 s. The intravenous contrast agent (100 mL of iopromide, 370 mg iodine per mL) (Ultravist 370; Bayer) was injected at a flow rate of 4 mL/s. The scan time delay was assessed using an automated bolus-tracking method with a monitoring section placed in the ascending aorta once the CT attenuation reached 120 HU (Hounsfield units). Axial CT angiographic images were reconstructed at a thickness of 0.67 mm.[17]

The point clouds representing the CAs and their adjacent parent arteries were obtained as shown in figure 1A. First, the original MRA or CTA DICOM (digital imaging and communications in medicine) data were imported to 3D Slicer (version 4.9.0; http://www.slicer.org), and the artery was segmented and reconstructed into a 3D model. Then, two radiologists independently segmented the aneurysm and its parent artery while blinded to the patient's information and the status of the aneurysm. Disparities regarding the aneurysm border were resolved by a third senior radiologist. Finally, the point clouds of aneurysm and its parent artery are obtained from the surface of the segmented 3D model. Details of the segmentation of the aneurysm and its parent artery are as follows: (1) the location of aneurysm was determined, and the region of interest (ROI) containing the aneurysm and its parent artery was cropped from the raw 3D images; (2) the local 3D artery model in the ROI was reconstructed by the single-threshold method[18]; (3) the 3D model was cleaned manually and only the aneurysm and a segment of its parent artery was preserved, and the preserved region of the parent artery was centered on the aneurysm and extended 3–5 mm to both sides of the artery; and (4) once the neck of aneurysm was determined, the preserved 3D artery was further segmented into the aneurysm part and the parent artery part along the aneurysm neck.

Point cloud neural network

As shown in figure 1B, the PC-NN model consists of two subnetworks. The first is a feature extraction network that extracts multiscale morphological features from the input point cloud, and the second is a rupture prediction network that calculates the probability of CA rupture based on the extracted morphological features and clinical features including sex, age, hypertension, hyperlipidemia, diabetes mellitus, smoking, drinking, multiplicity and location.

The morphological feature extraction network is composed of three set-abstraction levels proposed in PointNet++,[19] which aggregates features of the input point cloud layer by layer. The first two set-abstraction levels consist of three parallel branches with the same sampling rate but different grouping radii. In each branch, the sampling and grouping layer groups point clouds into smaller local regions, and then a three-layer fully connected network with shared weights across channels is applied to extract features from the input local regions. Finally, the features extracted from different branches are concatenated to obtain the multiscale point cloud morphological features. The final set-abstraction level has only one branch and aggregates all the features into a 1024-dimensional feature vector. Details of the network structure are provided in the online supplemental figure 1.

The rupture prediction network is a three-layer, fully connected network. The input layer contains 1035 neurons, which accept the extracted feature vectors and clinical features, and the output layer contains two neurons, whose outputs are mapped to (0, 1) by the softmax function to represent the probability of rupture.

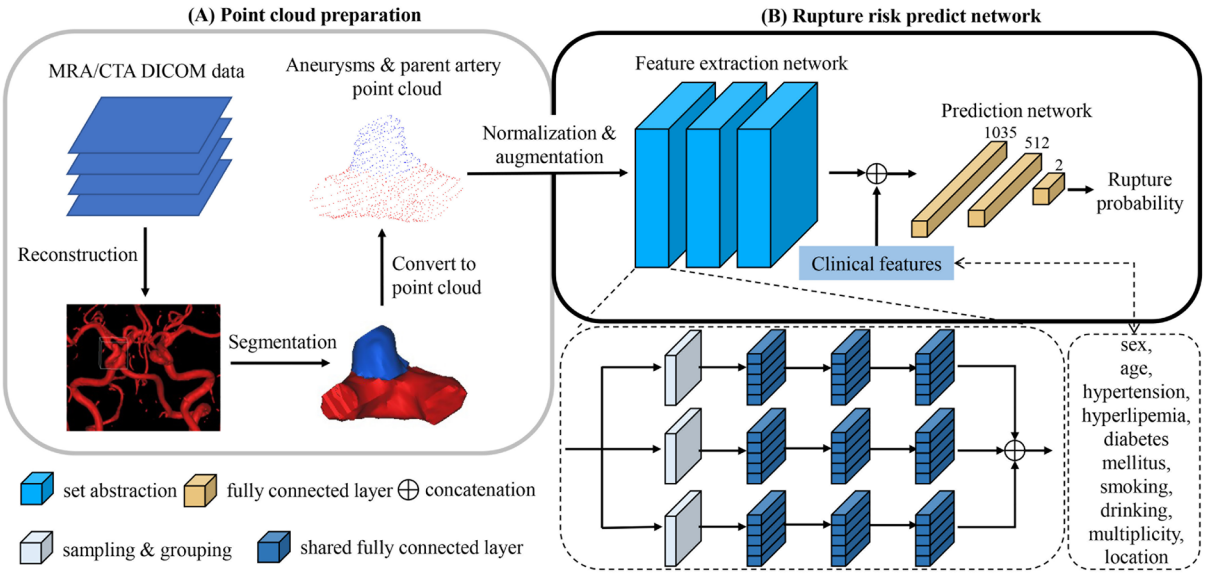

Figure 1 (A) Point cloud data preparation. First the artery is reconstructed into a 3D model and then the aneurysm and its parent artery are segmented. Finally the point clouds are obtained through sampling from the segmented mesh model. (B) Point cloud neural network structure. The network has a feature extraction network composed of three set abstraction layers and a prediction network composed of three fully connected layer. DICOM, digital imaging and communications in medicine.

Network training

Before being fed into PC-NN, each point cloud is downsampled to 1024 points, and the coordinates are normalized to within $[-1, 1]^3$ to obtain a point set of size 1024×3; then, the aneurysm and parent artery labels are further concatenated with the coordinates to obtain a point set of size 1024×4. During the PC-NN training, data augmentation is applied in an online manner, the whole point cloud is random rotated along x, y and z axis in the range of [−180°, 180°], and each point of the point cloud is random translated independently through adding a noise under Gaussian distribution N (0, 0.01).

The PC-NN was implemented in Python (version 3.6; Python Software Foundation, Wilmington, DE; https://www.python.org) and PyTorch (version 1.3.1; https://pytorch.org). Network parameters were trained from scratch using the Adam optimizer (learning rate=0.001, eta_1=0.9, beta_2=0.999, epsilon=0.00000001) on a 2 NVIDIA 2080Ti GPU for 100 epochs, and the learning rate was halved every 30 epochs. The training process took 39 min.

Radiomics features and traditional machine learning models

As previously reported,[7] PyRadiomics was adopted to extract nine morphological features from raw images, including Compactness1, Compactness2, SurfaceArea, SurfaceVolumeRatio, Sphericity, SphericalDisproportion, Maximum3DDiameter, Elongation and Flatness. Detailed information on these features is available in the documentation for PyRadiomics (http://PyRadiomics.readthedocs.io/en/latest/). The PyRadiomics-extracted features together with the clinical features were further normalized and fed to three traditional machine learning models, including a ridge regression model, a support vector machine (SVM) model and a neural network (NN) model, to predict aneurysm rupture. The ridge regression and SVM models are implemented with scikit-learn package,[20] and linear kernel of SVM is used. The NN is implemented with PyTorch. Parameters of ridge, SVM and NN are optimized by the least squares method or gradient decent algorithm with training data.

Evaluation

All of the aneurysms from the internal center were randomly divided into a non-overlapping training set (293 CAs, 70%) and a test set (125 CAs, 30%). For internal data, clinical characteristics, including sex, age, hypertension, hyperlipidemia, diabetes mellitus, smoking, and drinking, were included. The PC-NN models (with and without parent artery involvement) and radiomics models were trained and tested using the internal data set. Furthermore, the PC-NN model trained with only MRA or CTA internal data was also compared. Finally, the PC-NN and radiomics models were retrained without clinical features with all internal data and were tested in the external data set from five other centers. The receiver operating characteristic (ROC) curves of each model were built, and their areas under the curve (AUCs) were compared. The optimal cut-off points were calculated by the Youden index, and the sensitivity, specificity, positive predictive value (PPV), negative predictive value (NPV) and accuracy of each model under the optimal cut-off point in the ROC curve were obtained.[21]

Statistical analysis

Statistical analysis was performed with R (version 3.4.2; R Foundation for Statistical Computing, Vienna, Austria). The diagnostic performance of the models was evaluated using ROC analysis and pairwise comparisons of the AUC according to the DeLong method.[22] Differences in the clinical features and radiomics features between two groups were analyzed by Student's t test or Pearson χ^2 tests depending on the variable type. Statistical significance was defined as a two-tailed p value <0.05.

RESULTS

Patients

For internal data, a total of 418 CAs from 411 patients were included in the final analysis and were divided into training (n=293) and testing (n=125) sets, including 148 ruptured CAs (n=46 for MRA and n=102 for CTA) and 270 unruptured CAs (n=192 for MRA and n=78 for CTA) (online supplemental

Table 1 Comparison of clinical features between unruptured and ruptured aneurysms in patients in the internal data set

	Unruptured (n=270)	Ruptured (n=148)	P value	AUC (with location)	AUC (without location)
Sex (women)	174 (64.4%)	80 (54.1%)	0.024	0.544	0.632
Age	60.99±12.9	58.62±12.48	0.135	0.516	0.625
Hypertension	123 (45.6%)	86 (58.1%)	0.014	0.548	0.698
Hyperlipidemia	36 (13.3%)	12 (8.1%)	0.109	0.556	0.687
Diabetes mellitus	23 (8.5%)	9 (6.1%)	0.370	0.502	0.655
Smoking	30 (11.1%)	29 (19.6%)	0.017	0.554	0.658
Drinking	50 (18.5%)	38 (25.7%)	0.086	0.526	0.644
Multiple aneurysms	55 (20.4%)	14 (9.5%)	0.004	0.521	0.649
Location			<0.001	0.657	
ICA/PComA	199 (73.3%)	60 (40.5%)			
MCA	21 (7.8%)	15 (10.1%)			
ACA/AComA	50 (18.5%)	73 (49.3%)			

The data are presented as mean±SD or percentage.
Hypertension: blood pressure of 130/80 mm Hg or higher. Diabetes mellitus: HbA1c of 6.5% or higher. Hyperlipidemia: low-density lipoprotein cholesterol ≥160 mg/dL, hypertriglyceridemia ≥150 mg/dL, and/or low high-density lipoprotein cholesterol <40 mg/dL in men, <50 mg/dL in women. Smoking: continuous or cumulative smoking for 6 months or more.
ACA, anterior cerebral artery; AComA, anterior communicating artery; HbA1c, glycated hemoglobin; ICA, internal carotid artery; MCA, middle cerebral artery; PComA, posterior communicating artery.

table 1). A summary of the patient demographic and aneurysm information is provided in table 1. Male sex, hypertension and smoking were more prevalent in the ruptured aneurysm group (p=0.024, p=0.014, p=0.017, respectively), and aneurysms located in the ACA/AComA (49.3%) were more likely to rupture. For external data, a total of 258 CAs from 254 patients were prospectively included in the final test analysis, including 105 ruptured CAs (n=105 for CTA and n=0 for MRA) and 153 unruptured CAs (n=68 for MRA and n=85 for CTA). The inclusion flow chart is shown in figure 2.

Morphological features learned by the PC-NN model

In order to understand the meaning of features learned by PC-NN, the 1024-dimensional morphological features learned by PC-NN are reduced to 3D features with principal component analysis (PCA). The results are shown in the online supplemental figure 2. The histogram on the left shows the distribution of three features in ruptured and unruptured aneurysms after PCA dimensionality reduction. According to the size of eigenvalues, we visualized some aneurysms. According to the visualization results, it can be seen that smaller aneurysms in feature 1 are mostly located at the bifurcation of blood vessels, and the size of aneurysms is larger. In feature 2, small aneurysms are more irregular in shape. In feature 3, small aneurysms have a smaller angle to the parent artery.

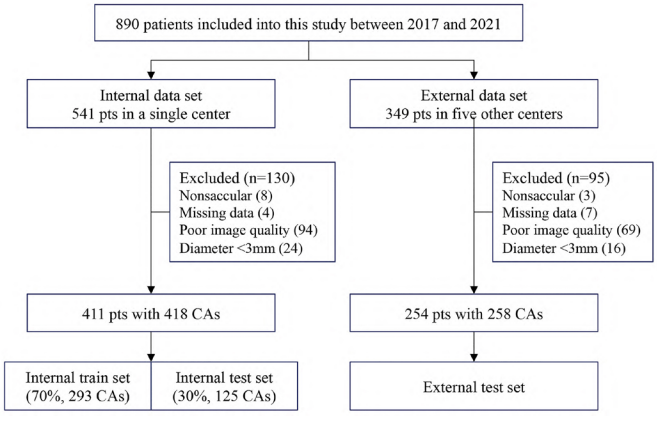

Figure 2 Flow chart of patient selection. CAs, cerebral aneurysms.

Parent artery involvement increases the prediction accuracy by the PC-NN model

When the point clouds representing both the aneurysm and its parent artery were used to predict aneurysm rupture, the AUC of the resulting ROC curve was 0.913 (95% CI 0.861 to 0.966), which was significantly higher than the AUC value (0.851, 95% CI 0.783 to 0.920; p=0.041) when point clouds represented only the aneurysm (figure 3A). The sensitivity and specificity at the optimal cut-off value of 0.754 were 89.4% (95% CI 80.5% to 98.2%) and 81.8% (95% CI 73.2% to 90.4%), respectively, when PC-NN models had parent artery involvement (table 2).

MRA source data increase the prediction accuracy by PC-NN model

MRA (n=238) and CTA (n=180) internal data were separately used to train (70%) and test (30%) the PC-NN models. The resulting ROC curves obtained with the test set showed a higher AUC value for the model trained with the MRA source data (0.936, 95% CI 0.865 to 1.000) than for the model trained with the CTA source data (0.824, 95% CI 0.702 to 0.947; p=0.043) (table 2). The optimal cut-off value for the PC-NN model using MRA source data was 0.756, with a sensitivity and specificity of 86.7% (95% CI 69.5% to 100.0%) and 91.1% (95% CI 83.6% to 98.5%), respectively. The optimal cut-off value for the PC-NN model using CTA source data was 0.499, with a sensitivity and specificity of 78.1% (95% CI 63.8% to 92.4%) and 85.7% (95% CI 70.7% to 100.0%), respectively (figure 3B).

Prediction accuracy by PC-NN model was superior to radiomics models

In the internal data set, the morphological features extracted by using PyRadiomics are shown in online supplemental table 2, which revealed significant differences between the ruptured and unruptured aneurysms. Ruptured aneurysms had larger values for SurfaceArea (p<0.001), SurfaceVolumeRatio (p<0.001), SphericalDisproportion (p=0.004) and Maximum3DDiameter (p<0.001), but smaller values for Compactness1 (p=0.007), Compactness2 (p=0.013), Sphericity (p=0.006), and Flatness (p<0.001) than unruptured aneurysms. These results indicate that larger and irregularly-shaped aneurysms were more likely to rupture. The AUCs of the ridge regression, SVM and NN models were 0.803 (95% CI 0.725 to 0.882), 0.788 (95% CI 0.704 to 0.872) and 0.805 (95% CI 0.727 to 0.883), respectively, and were not significantly different (table 3, online supplemental table 3, figure 3C).

When only the aneurysm point cloud was used, the PC-NN model had an AUC similar to that of the three other radiomics models (p>0.05) in predicting CA rupture. However, the prediction performance of the PC-NN model trained with the aneurysm and parent artery point cloud data (AUC=0.913, 95% CI 0.861 to 0.966) was superior to that of the other radiomics models (p<0.05) (online supplemental table 3).

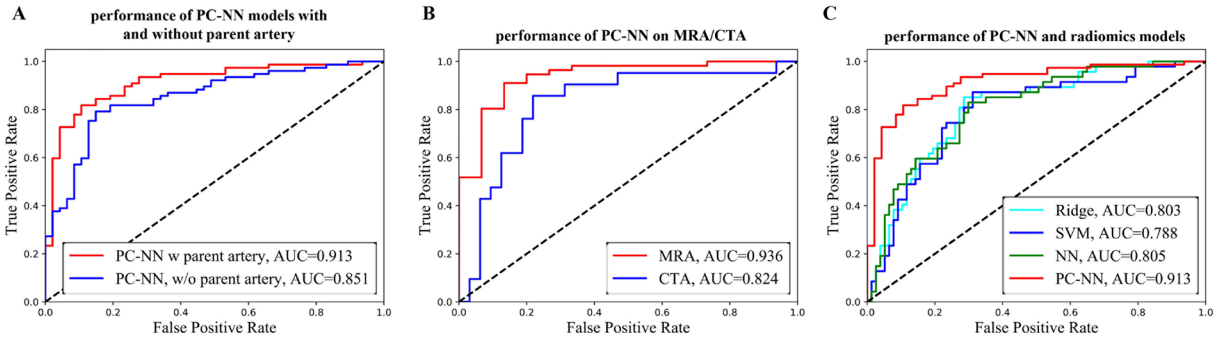

Figure 3 The ROC curves of PC-NN and radiomics models in the internal test data set. (A) Performance of the PC-NN model with and without parent artery involvement in the internal test data set. (B) Performance of the PC-NN model trained separately with the internal MRA and CTA data sets. (C) Performance of PC-NN with parent artery involvement and different machine learning models based on radiomics features in the internal test dataset. AUC, area under the curve, CTA, CT angiography; MRA, MR angiography; NN, neural network; PC-NN, point cloud neural network; ROC, receiver operating characteristic; SVM, support vector machine.

Prediction by different models in patients from external centers

PC-NN and radiomics models were verified to predict aneurysm rupture in prospectively included patients from external centers (n=254). The AUC of PC-NN was 0.835 (95% CI 0.786 to 0.884), which was also significantly higher than that of the ridge (AUC=0.692, 95% CI 0.625 to 0.758; p<0.001), SVM (AUC=0.701, 95% CI 0.635 to 0.766; p<0.001) and NN (AUC=0.681, 95% CI 0.614 to 0.747; p<0.001) (figure 4E, table 3).

DISCUSSION

In the present study, we applied a PC-NN model to predict aneurysm rupture, and its feasibility and accuracy were further investigated by using different data sources and compared with those of traditional radiomics-based methods. Our preliminary results show that the PC-NN was an optimal model for predicting aneurysm rupture; additionally, we found that (1) the PC-NN model trained with point clouds representing both the aneurysm and its parent artery had a higher AUC than that trained with only aneurysm point clouds; (2) the PC-NN model achieved a higher AUC value when trained and tested with MRA data than with CTA data; and (3) the PC-NN model was superior to other radiomics models in predicting aneurysm rupture in both internal and external test data.

Traditional morphological features are manually measured, and the measurements may differ among raters and projections.[7 23] Radiomics-based methods can be used to automatically measure morphological features directly from 3D images and reduce the subjective effect in the measurements. However, these radiomics-based methods can only extract several low-level morphological features, such as the diameter, volume and surface area of the aneurysm.[10 11 24] Compared with traditional morphological analysis methods based on manual measurement and radiomics-based methods, our PC-NN is capable of deep learning and can learn 1024 complex and high-level morphological features from vascular diseases. The visualization results showed that the learned 1024-dimensional features were related to aneurysm size, location, shape and angle. Although manually designed features are also related to these factors, the much higher dimensional features learned by PC-NN could capture smaller morphological differences between ruptured and unruptured aneurysms and is the key for PC-NN to exceed the method of radiomics. In our study, after extraction of a wealth of morphological features of aneurysms and their parent arteries, the PC-NN model achieved a significantly higher AUC in both the internal and external data sets than three traditional radiomics-based models, including ridge regression (internal p=0.019, external p<0.001), SVM (internal p=0.013, external p<0.001) and NN (internal p=0.023, external p<0.001) models, which only extracted radiomics features from the aneurysms.

More recently, a few studies reported predicting aneurysm rupture based on deep learning using convolutional neural networks (CNNs). Heung *et al* projected the extracted ROIs of aneurysms and their parent arteries into 2D images for 272 aneurysms and constructed a CNN to assess their rupture probability, achieving an AUC of 0.755.[25] Ahn *et al* used a similar image projection method and further adopted a multiview CNN to predict rupture with an accuracy of 81.72%.[26] Compared with these CNN-based deep learning methods, PC-NN has more

Table 2 Comparison of prediction performance between PC-NN models in internal test data set

	Sensitivity (%)	Specificity (%)	PPV (%)	NPV (%)	Accuracy (%)	AUC	P value
PC-NN, with artery	89.4 (80.5–98.2)	81.8 (73.2–90.4)	92.6 (86.4–98.9)	75.0 (63.7–86.3)	84.7 (84.5–84.9)	0.913 (0.861–0.966)	0.041
PC-NN, without artery	85.1 (74.9–95.3)	79.2 (70.2–88.3)	89.7 (82.5–96.9)	71.4 (59.6–83.3)	81.5 (81.2–81.7)	0.851 (0.783–0.920)	
PC-NN, with clinical feature	89.4 (80.5–98.2)	81.8 (73.2–90.4)	92.6 (86.4–98.9)	75.0 (63.7–86.3)	84.7 (84.5–84.9)	0.913 (0.861–0.966)	0.341
PC-NN, without clinical feature	95.7 (90.0–100.0)	62.3 (51.5–73.2)	96.0 (90.6–100.0)	60.8 (49.7–71.9)	75.0 (74.7–75.3)	0.876 (0.817–0.934)	
PC-NN, MRA	86.7 (69.5–100.0)	91.1 (83.6–98.5)	96.2 (91.1–100.0)	72.2 (51.5–92.9)	90.1 (89.9–90.4)	0.936 (0.865–1.000)	0.043
PC-NN, CTA	78.1 (63.8–92.4)	85.7 (70.7–100.0)	72.0 (54.4–89.6)	89.3 (77.8–100.0)	81.1 (80.6–81.7)	0.824 (0.702–0.947)	

The data are presented as the mean±SD or percentage.
AUC, area under the curve; CTA, CT angiography; MRA, MR angiography; NPV, negative predictive value; PC-NN, point cloud neural network; PPV, positive predictive value.;

Table 3 Comparison of prediction performance between the PC-NNs and radiomics models in internal and external test sets

	Test set	Sensitivity (%)	Specificity (%)	PPV (%)	NPV (%)	Accuracy (%)	AUC	P value
PC-NN, with artery	Internal test	89.4 (80.5–98.2)	81.8 (73.2–90.4)	92.6 (86.4–98.9)	75.0 (63.7–86.3)	84.7 (84.5–84.9)	0.913 (0.861–0.966)	
Ridge regression	Internal test	85.1 (74.9–95.3)	71.4 (61.3–81.5)	64.5 (52.6–76.4)	88.7 (80.8–96.6)	76.6 (76.3–76.9)	0.803 (0.725–0.882)	0.019
SVM	Internal test	87.2 (77.7–96.8)	68.8 (58.5–79.2)	63.1 (51.3–74.8)	89.8 (82.1–97.5)	75.8 (75.5–76.1)	0.788 (0.704–0.872)	0.013
NN	Internal test	83.0 (72.2–93.7)	70.1 (59.9–80.4)	62.9 (50.9–74.9)	87.1 (78.8–95.4)	75.0 (74.7–75.3)	0.805 (0.727–0.883)	0.023
PC-NN, with artery	External test	79.1 (72.6–85.5)	77.1 (69.1–85.2)	83.4 (77.4–89.5)	71.7 (63.4–80.0)	78.3 (78.2–78.4)	0.835 (0.786–0.884)	
Ridge regression	External test	65.7 (56.6–74.8)	68.6 (61.3–76.0)	59.0 (50.1–67.9)	74.5 (67.3–81.7)	67.4 (67.3–67.6)	0.692 (0.625–0.758)	<0.001
SVM	External test	64.8 (55.6–73.9)	69.3 (62.0–76.6)	59.1 (50.1–68.1)	74.1 (66.9–81.3)	67.4 (67.3–67.6)	0.701 (0.635–0.766)	<0.001
NN	External test	61.0 (51.6–70.3)	71.2 (64.1–78.4)	59.3 (50.0–68.5)	72.7 (65.5–79.8)	67.1 (66.9–67.2)	0.681 (0.614–0.747)	<0.001

The data are presented as the mean±SD or percentage.
AUC, area under the curve; NN, neural network; NPV, negative predictive value; PC-NN, point cloud neural network; PPV, positive predictive value; SVM, support vector machine.

advantages. First, the PC-NN learns from the 3D coordinates of the aneurysm instead of from projected 2D images, which ensures that the network learns the original morphological features. Second, as images obtained from different modalities have very large domain gaps, most deep learning methods cannot generalize well from one modality to another.[27] However, the point clouds extracted from different modalities are very similar, indicating that the trained PC-NN would have better cross modality performance than image-based CNNs. This advantage not only enables application of the trained network to broader scenarios but also fulfills the need for deep neural networks for large amounts of data. Finally, the number of model parameters of the PC-NN is much smaller than that of the CNN, and the training and inferencing speeds of the PC network are higher.[15]

Compared with the PC-NN trained with only aneurysm data, the PC-NN trained with both aneurysm and parent artery data achieved a better prediction performance. Our results showed that after including the point cloud of the parent arteries, the AUC of the PC-NN model reached 0.913, which was significantly higher than that of the PC-NN model trained only with the aneurysm point cloud (AUC=0.851, p=0.041). We speculate that there are two advantages in extracting the morphological features of the adjacent parent artery. First, PC-NN may extract richer morphological features, such as the angle between the aneurysm and its parent artery or the diameters of the parent artery, which have been reported to be associated with aneurysm rupture.[28] Second, previous research has indicated that deep learning models can directly learn blood flow patterns from aneurysm images, and hemodynamic parameters, including velocity and pressure fields, can be directly recognized by deep neural networks rather than through blood flow simulations.[29] Similarly, PC-NN may have the potential to learn hemodynamic factors from point cloud data when the point clouds of both the aneurysm and parent artery are retained.

Although there is no modality difference between MRA and CTA images after they have been reconstructed into point clouds, the point clouds reconstructed from MRA are denser than those reconstructed from CTA due to the higher resolution of the source images from the former. Therefore, we compared the performance of the PC-NN model when trained

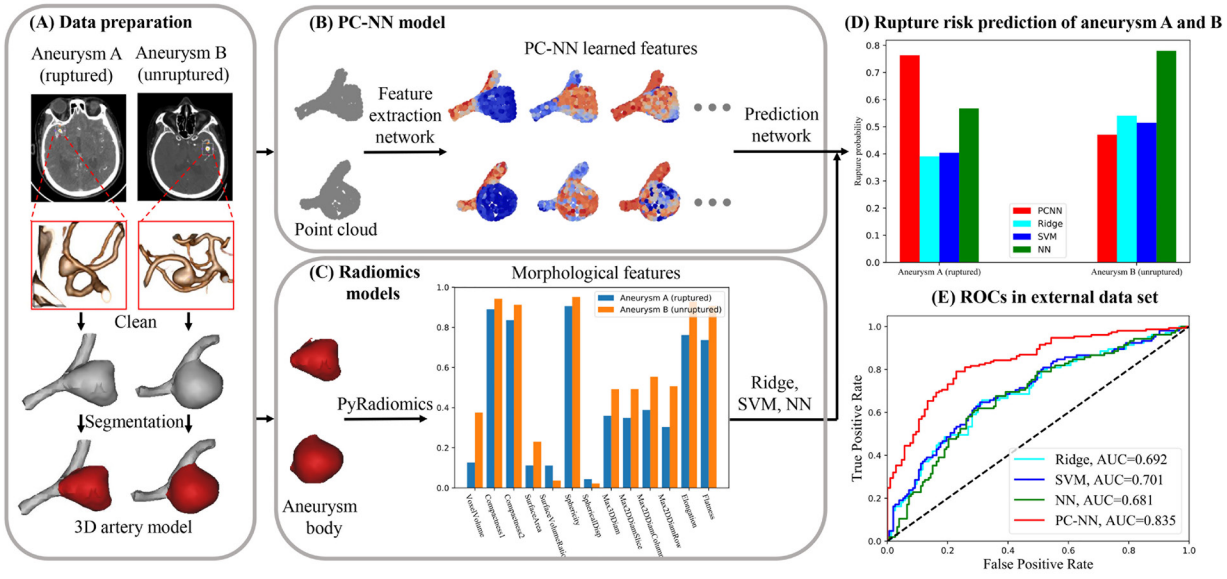

Figure 4 (A) The data preparation flow using a ruptured (aneurysm A) and an unruptured (aneurysm B) MCA aneurysm in an external data set to perform rupture prediction using both PC-NN and radiomics models. (B) The trained PC-NN network made predictions based on thousands of features from both the aneurysm body and parent artery. (C) Radiomics models made predictions based on 13 morphological features of the aneurysm body. (D) Prediction results of aneurysms A and B indicated that the PC-NN model was more accurate than the radiomics models. (E) Comparison of prediction results among the PC-NN and radiomics models with respect to the whole external data set. AUC, area under the curve; MCA, middle cerebral artery; NN, neural network; PC-NN, point cloud neural network, ROC, receiver operating characteristic; SVM, support vector machine.

with each modality separately and found that the model trained with MRA achieved a higher AUC than the model trained with CTA (p=0.043). The superior performance of the MRA data arises from its higher resolution, which can better reflect the aneurysm shape and lead to the acquisition of more detailed information. Based on these results, it is suggested that MRA data be used to further increase the accuracy of rupture prediction.

With the advancement of artificial intelligence methods, deep learning models have been introduced to the medical area to achieve great success. CNNs have been adopted for aneurysm detection and continue to show improved performance.[30] Applying the PC-NN model to clinical CA rupture prediction may potentially be more advantageous than the application of the CNN. First, the PC-NN can automatically process massive amounts of data and use them to make predictions, leading to high prediction efficiency and avoiding subjective effects in measurements. Second, compared with radiomics-based methods, the PC-NN demonstrated superior prediction performance, and the ability to accurately predict rupture could facilitate treatment optimization and lead to better outcomes. Third, the trained PC-NN makes predictions based on point clouds and thus can be applied to different modality data, including MRA and CTA.

LIMITATIONS

This study has some limitations. First, it was a retrospective study. Second, a relatively high percentage of patients were excluded due to inaccurate aneurysm and artery segmentation, which may have reduced the prediction performance of our model in the real world. Third, the morphology of aneurysms may change after rupture, and this post-rupture morphology is not an adequate surrogate for the pre-rupture morphology. Finally, as our data set is 3D data, other deep learning methods based on 2D-CNN were not used for comparison with our PC-NN model.

CONCLUSIONS

In this study, a model for the prediction of aneurysm rupture from CTA or MRA images based on a point cloud neural network was devised and evaluated. The PC-NN model learned to extract morphological features from both aneurysms and their parent arteries and achieved better prediction performance than conventional machine learning models based on radiomics features. The PC-NN model may thus become a supportive and complementary tool to provide individualized treatment plans for patients with CA in the clinic.

Author affiliations
[1]Digital Medical Research Center and also with the Shanghai Key Laboratory of Medical Image Computing and Computer Assisted Intervention, Fudan University, Shanghai, China
[2]Department of Radiology, Shanghai Jiao Tong University Affiliated Sixth People's Hospital, Shanghai, China
[3]Department of Radiology, Shanghai Tenth People's Hospital, Tongji University, Shanghai, China
[4]Department of Interventional Radiology, First Affiliated Hospital of Zhengzhou University, Zhengzhou, Henan, China
[5]Department of Neurosurgery, The Affiliated Drum Tower Hospital of Nanjing University Medical School, Nanjing, China
[6]Department of Nuclear Medicine, The Affiliated Drum Tower Hospital of Nanjing University Medical School, Nanjing, China
[7]Department of Neurosurgery, Anhui Medical University Affiliated First Hospital, Hefei, China
[8]Department of Neurosurgery, Renji Hospital, Shanghai Jiao Tong University School of Medicine, Shanghai, China

Contributors XL, JW: Acquisition of data, study concept and design, analysis and interpretation of data and drafting of the manuscript. MW, YZ: Study concept and design, critical revision of the manuscript for important intellectual content, and study supervision. XL, LY, XC, JH, JL, BZ, GH: Acquisition of data, revision of the manuscript. XL, JW: Statistical analysis. YZ: Responsible for the overall content as guarantor

Funding Supported by Shanghai Municipal Education Commission (Gaofeng Clinical Medicine grant support no. 20152528) and Shanghai Jiao Tong University Medical and Research Program (ZH2018ZDA19).

Competing interests None declared.

Patient consent for publication Consent obtained from parent(s)/guardian(s)

Ethics approval This study involves human participants and was approved by the ethics committees of the following hospitals: (1) Shanghai Jiao Tong University Affiliated Sixth People's Hospital (2018-041); (2) Shanghai Tongji University Affiliated Tenth People's Hospital (SHSY-IEC-4.1/21-324/01); (3) The First Affiliated Hospital of Zhengzhou University (2015-03); (4) Nanjing University Affiliated Gulou Hospital (2020-041-01); (5) Anhui Medical University Affiliated First Hospital (PJ2021-08-41); (6) Medical School of Shanghai Jiaotong University Affiliated Renji Hospital (2017-093). Participants gave informed consent to participate in the study before taking part.

Provenance and peer review Not commissioned; externally peer reviewed.

Data availability statement Data are available upon reasonable request. Not applicable.

ORCID iDs
Bing Zhao http://orcid.org/0000-0002-5562-0392
Yueqi Zhu http://orcid.org/0000-0001-5476-9075

REFERENCES

1 Backes D, Rinkel GJE, Laban KG, *et al*. Patient- and aneurysm-ppecific risk factors for intracranial aneurysm growth: a systematic review and meta-analysis. *Stroke* 2016;47:951–7.
2 Wang J, Wei L, Lu H, *et al*. Roles of inflammation in the natural history of intracranial saccular aneurysms. *J Neurol Sci* 2021;424:117294.
3 Sun L, Wang J, Li M, *et al*. The contribution of wall shear stress insult to the growth of small unruptured cerebral aneurysms in longitudinal 3D-TOF-MRA. *J Neurol Sci* 2020;413:116798.
4 UCAS Japan Investigators, Morita A, Kirino T, *et al*. The natural course of unruptured cerebral aneurysms in a Japanese cohort. *N Engl J Med* 2012;366:2474–82.
5 Chen Y, Xing H, Lin B, *et al*. Morphological risk model assessing anterior communicating artery aneurysm rupture: development and validation. *Clin Neurol Neurosurg* 2020;197:106158.
6 Detmer FJ, Chung BJ, Jimenez C, *et al*. Associations of hemodynamics, morphology, and patient characteristics with aneurysm rupture stratified by aneurysm location. *Neuroradiology* 2019;61:275–84.
7 Liu Q, Jiang P, Wu J, *et al*. The morphological and hemodynamic characteristics of the intraoperative ruptured aneurysm. *Front Neurosci* 2019;13:233.
8 Xu W-D, Wang H, Wu Q, *et al*. Morphology parameters for rupture in middle cerebral artery mirror aneurysms. *J Neurointerv Surg* 2020;12:858–61.
9 van Griethuysen JJM, Fedorov A, Parmar C, *et al*. Computational radiomics system to decode the radiographic phenotype. *Cancer Res* 2017;77:e104–7.
10 Ludwig CG, Lauric A, Malek JA, *et al*. Performance of radiomics derived morphological features for prediction of aneurysm rupture status. *J Neurointerv Surg* 2021;13:neurintsurg-2020-016808.
11 Liu Q, Jiang P, Jiang Y, *et al*. Prediction of aneurysm stability using a machine learning model based on PyRadiomics-derived morphological features. *Stroke* 2019;50:2314–21.
12 Rahman M, Smietana J, Hauck E, *et al*. Size ratio correlates with intracranial aneurysm rupture status: a prospective study. *Stroke* 2010;41:916–20.
13 Lauric A, Miller EL, Baharoglu MI, *et al*. 3D shape analysis of intracranial aneurysms using the writhe number as a discriminant for rupture. *Ann Biomed Eng* 2011;39:1457–69.
14 Piccinelli M, Steinman DA, Hoi Y, *et al*. Automatic neck plane detection and 3D geometric characterization of aneurysmal sacs. *Ann Biomed Eng* 2012;40:2188–211.

15 CR Q, Su H, Mo K. Pointnet: deep learning on point sets for 3D classification and segmentation. Paper presented at 2017 IEEE conference on computer vision and pattern recognition; July 21-26; 2017; Honolulu, USA. Available: https://openaccess.thecvf.com/content_cvpr_2017/papers/Qi_PointNet_Deep_Learning_CVPR_2017_paper.pdf [Accessed 1 Sep 2020].
16 Li M, Zhu Y, Song H, *et al*. Subarachnoid hemorrhage in patients with good clinical grade: accuracy of 3.0-T MR angiography for detection and characterization. *Radiology* 2017;284:191–9.
17 Wei L, Zhu Y, Deng J, *et al*. Visualization of thrombus enhancement on thin-slab maximum intensity projection of CT angiography: an imaging sign for predicting stroke source and thrombus compositions. *Radiology* 2021;298:374–81.
18 Hoogeveen RM, Bakker CJ, Viergever MA. Limits to the accuracy of vessel diameter measurement in MR angiography. *J Magn Reson Imaging* 1998;8:1228–35.
19 C R Q, Yi L, Su H. PointNet++: deep hierarchical feature learning on point sets in a metric space. Paper presented at 31st International Conference on Neural Information Processing Systems; December 4-9; 2017; Long Beach, USA. Available: https://proceedings.neurips.cc/paper/2017/file/d8bf84be3800d12f74d8b05e9b89836f-Paper.pdf [Accessed 1 Sept 2020].
20 Pedregosa F, Varoquaux G, Gramfort A. Scikit-learn: machine learning in python. *J Mach Learn Res* 2011;12:2825–30.
21 Detmer FJ, Chung BJ, Mut F, *et al*. Development and internal validation of an aneurysm rupture probability model based on patient characteristics and aneurysm location, morphology, and hemodynamics. *Int J Comput Assist Radiol Surg* 2018;13:1767–79.
22 DeLong ER, DeLong DM, Clarke-Pearson DL. Comparing the areas under two or more correlated receiver operating characteristic curves: a nonparametric approach. *Biometrics* 1988;44:837–45.
23 Duan Z, Li Y, Guan S, *et al*. Morphological parameters and anatomical locations associated with rupture status of small intracranial aneurysms. *Sci Rep* 2018;8:6440.
24 Ou C, Chong W, Duan C-Z, *et al*. A preliminary investigation of radiomics differences between ruptured and unruptured intracranial aneurysms. *Eur Radiol* 2021;31:2716–25.
25 Kim HC, Rhim JK, Ahn JH, *et al*. Machine learning application for rupture risk assessment in small-sized intracranial aneurysm. *J Clin Med* 2019;8. doi:10.3390/jcm8050683. [Epub ahead of print: 15 05 2019].
26 Ahn JH, Kim HC, Rhim JK, *et al*. Multi-view convolutional neural networks in rupture risk assessment of small, unruptured intracranial aneurysms. *J Pers Med* 2021;11. doi:10.3390/jpm11040239. [Epub ahead of print: 24 03 2021].
27 Yang J, Dvornek NC, Zhang F, *et al*. Unsupervised domain adaptation via disentangled representations: application to cross-modality liver segmentation. *Med Image Comput Comput Assist Interv* 2019;11765:255–63.
28 İdil Soylu A, Ozturk M, Akan H. Can vessel diameters, diameter ratios, and vessel angles predict the development of anterior communicating artery aneurysms: a morphological analysis. *J Clin Neurosci* 2019;68:250–5.
29 Raissi M, Yazdani A, Karniadakis GE. Hidden fluid mechanics: learning velocity and pressure fields from flow visualizations. *Science* 2020;367:1026–30.
30 Ueda D, Yamamoto A, Nishimori M, *et al*. Deep learning for MR angiography: automated detection of cerebral aneurysms. *Radiology* 2019;290:187–94.